8

Dielectrophoretic Traps for Cell Manipulation

Joel Voldman

Department of Electrical Engineering, Room 36-824, Massachusetts Institute of Technology Cambridge, MA 02139

8.1. INTRODUCTION

One of the goals of biology for the next fifty years is to understand how cells work. This fundamentally requires a diverse set of approaches for performing measurements on cells in order to extract information from them. Manipulating the physical location and organization of cells or other biologically important particles is an important part in this endeavor. Apart from the fact that cell function is tied to their three-dimensional organization, one would like ways to grab onto and position cells. This lets us build up controlled multicellular aggregates, investigate the mechanical properties of cells, the binding properties of their surface proteins, and additionally provides a way to move cells around. In short, it provides physical access to cells that our fingers cannot grasp.

Many techniques exist to physically manipulate cells, including optical tweezers [78], acoustic forces [94], surface modification [52], etc. Electrical forces, and in particular dielectrophoresis (DEP), are an increasingly common modality for enacting these manipulations. Although DEP has been used successfully for many years to separate different cell types (see reviews in [20, 38]), in this chapter I focus on the use of DEP as "electrical tweezers" for manipulating individual cells. In this implementation DEP forces are used to trap or spatially confine cells, and thus the chapter will focus on creating such traps using these forces. While it is quite easy to generate forces on cells with DEP, it is another thing altogether to obtain predetermined quantitative performance. The goal for this chapter is to help others develop an approach to designing these types of systems. The focus will be on trapping cells—which at times are generalized to "particles"—and specifically mammalian

cells, since these are more fragile than yeast or bacteria and thus are in some ways more challenging to work with.

I will start with a short discussion on what trapping entails and then focus on the forces relevant in these systems. Then I will discuss the constraints when working with cells, such as temperature rise and electric field exposure. The last two sections will describe existing trapping structures as well as different approaches taken to measure the performance of those structures. The hope is that this overview will give an appreciation for the forces in these systems, what are the relevant design issues, what existing structures exist, and how one might go about validating a design. I will not discuss the myriad other uses of dielectrophoresis; these are adequately covered in other texts [39, 45, 60] and reviews.

8.2. TRAPPING PHYSICS

8.2.1. Fundamentals of Trap Design

The process of positioning and physically manipulating particles—cells in this case—is a trapping process. A trap uses a set of confining forces to hold a particle against a set of destabilizing forces. In this review, the predominant confining force will be dielectrophoresis, while the predominant destabilizing forces will be fluid drag and gravity. The fundamental requirement for any deterministic trap is that it creates a region where the net force on the particle is zero. Additionally, the particle must be at a stable zero, in that the particle must do work on the force field in order to move from that zero [3]. This is all codified in the requirement that $\mathbf{F}_{\mathbf{net}} = 0, \mathbf{F}_{\mathbf{net}} \cdot d\mathbf{r} < 0$ at the trapping point, where $\mathbf{F}_{\mathbf{net}}$ is the net force and $d\mathbf{r}$ is an increment in any direction.

The design goal is in general to create a particle trap that meets specific requirements. These requirements might take the form of a desired trap strength or maximum flowrate that trapped particles can withstand, perhaps to meet an overall system throughput specification. For instance, one may require a minimum flowrate to replenish the nutrients around trapped cells, and thus a minimum flowrate against which the cells must be trapped. When dealing with biological cells, temperature and electric-field constraints are necessary to prevent adverse effects on cells. Other constraints might be on minimum chamber height or width—to prevent particle clogging—or maximum chamber dimensions—to allow for proximate optical access. In short, *predictive quantitative* trap design. Under the desired operating conditions, the trap must create a stable zero, and the design thus reduces to ensuring that stable zeros exist under the operating conditions, and additionally determining under what conditions those stable zeros disappear (i.e., the trap releases the particle).

Occasionally, it is possible to analytically determine the conditions for stable trapping. When the electric fields are analytically tractable and there is enough symmetry in the problem to make it one-dimensional, this can be the best approach. For example, one can derive an analytical expression balancing gravity against an exponentially decaying electric field, as is done for field-flow fractionation [37]. In general, however, the fields and forces are too complicated spatially for this approach to work. In these cases, one can numerically calculate the fields and forces everywhere in space and find the net force ($\mathbf{F}_{\mathbf{net}}$) at each point, then find the zeros.

A slightly simpler approach exists when the relevant forces are conservative. In this case one can define scalar potential energy functions U whose gradient gives each force (i.e., $\mathbf{F} = -\nabla U$). The process of determining whether a trap is successfully confining the particle then reduces to determining whether any spatial minima exist within the trap. This approach is nice because energy is a scalar function and thus easy to manipulate by hand and on the computer.

In general, a potential energy approach will have limited applicability because dissipation is usually present. In this case, the energy in the system depends on the specifics of the particle motion—one cannot find a U that will uniquely define $\mathbf{F}$. In systems with liquid flow, for example, an energy-based design strategy cannot be used because viscous fluid flow is dissipative. In this case, one must use the vector force-fields and find stable zeroes.

In our lab, most modeling incorporates a range of approaches spanning analytical, numerical, and finite-element modeling. In general, we find it most expedient to perform finite-element modeling only when absolutely necessary, and spend most of the design combining those results with analytical results in a mixed-numerical framework run on a program such as Matlab© (Mathworks, Natick, MA). Luckily, one can run one or two finite-element simulations and then use simple scaling laws to scale the resulting data appropriately. For instance, the linearity of Laplace's equation means that after solving for the electric fields at one voltage, the results can be linearly scaled to other voltages. Thus, FEA only has to be repeated when the geometry scales, if at all.

To find the trapping point (and whether it exists), we use MATLAB to compute the three isosurfaces where each component of the net force (F_x, F_y, F_z) is zero. This process is shown in Figure 8.1 for a planar quadrupole electrode structure. Each isosurface—the three-dimensional analog of a contour line—shows where in space a single component of the force is zero. The intersection of all three isosurfaces thus represents points where all three force components, and thus the net force, is zero. In the example shown in Figure 8.1,B–D, increasing the flowrate changes the intersection point of the isosurfaces, until at some threshold flowrate (Figure 8.1D), the three isosurfaces cease to intersect, and the particle is no longer held; the strength of the trap has been exceeded [83]. In this fashion we can determine the operating characteristics (e.g., what voltage is needed to hold a particular cell against a particular flow) and then whether those characteristics meet the system requirements (exposure of cells to electric fields, for instance).

A few caveats must be stated regarding this modeling approach. First, the problem as formulated is one of determining under what conditions an already trapped particle will remain trapped; I have said nothing about how to get particles in traps. Luckily this is not a tremendous extension. Particle inertia is usually insignificant in microfluidic systems, meaning that particles will follow the streamlines of the force field. Thus, with numerical representations of the net force, one can determine, given a starting point, where that particle will end up. Matlab in fact has several commands to do this (e.g., streamline). By placing test particles in different initial spots, it is possible to determine the region from within which particles will be drawn to the trap.

Another implicit assumption is that only one particle will be in any trap, and thus that particle-particle interactions do not have to be dealt with. In actuality, designing a trap that will only hold one particle is quite challenging. To properly model this, one must account for the force perturbations created when the first particle is trapped; the second particle sees a force field modified by the first particle. While multiple-particle modeling is still largely

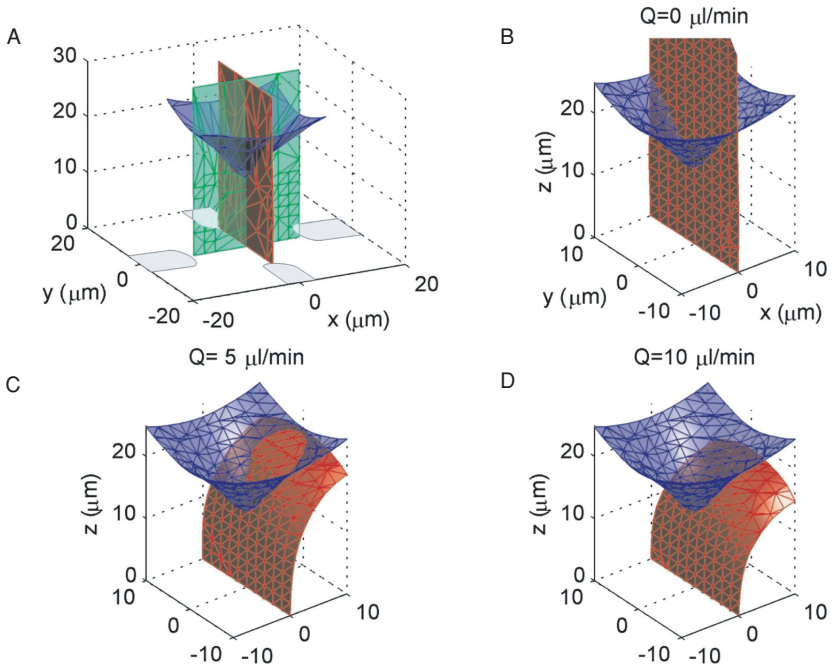

FIGURE 8.1. Surfaces of zero force describe a trap. **(A)** Shown are the locations of planar quadrupole electrodes along with the three isosurfaces where one component of the force on a particle is zero. The net force on the particle is zero where the three surfaces intersect. **(B–D)** As flow increases from left to right, the intersection point moves. The third isosurface is not shown, though it is a vertical sheet perpendicular to the $F_x = 0$ isosurface. **(D)** At some critical flow rate, the three isosurfaces no longer intersect and the particle is no longer trapped.

unresolved, the single-particle approach presented here is quite useful because one can, by manipulating experimental conditions, create conditions favorable for single-particle trapping, where the current analysis holds.

Finally, we have constrained ourselves to deterministic particle trapping. While appropriate for biological cells, this assumption starts to break down as the particle size decreases past $\sim$1μm because Brownian motion makes trapping a probabilistic event. Luckily, as nanoparticle manipulation has become more prevalent, theory and modeling approaches have been determined. The interested reader is referred to the monographs by Morgan and Green [60] and Hughes [39].

8.2.2. Dielectrophoresis

The confining force that creates the traps is dielectrophoresis. Dielectrophoresis (DEP) refers to the action of a body in a non-uniform electric field when the body and the surrounding medium have different polarizabilities. DEP is easiest illustrated with reference to Figure 8.2. On the left side of Figure 8.2, a charged body and a neutral body (with different permittivity than the medium) are placed in a uniform electric field. The charged body feels a force, but the neutral body, while experiencing an induced dipole, does not feel a net

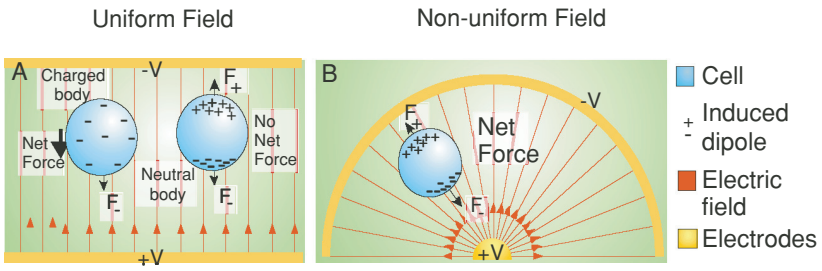

FIGURE 8.2. Dielectrophoresis. The left panel (A) shows the behavior of particles in uniform electric fields, while the right panel shows the net force experienced in a non-uniform electric field (B).

force. This is because each half of the induced dipole feels opposite and equal forces, which cancel. On the right side of Figure 8.2, this same body is placed in a non-uniform electric field. Now the two halves of the induced dipole experience a different force magnitude and thus a net force is produced. This is the dielectrophoretic force.

The force in Figure 8.2, where an induced dipole is acted on by a non-uniform electric field, is given by [45]

$$\mathbf{F}_{dep} = 2\pi\varepsilon_m R^3 \mathrm{Re}[\underline{CM}(\omega)] \cdot \nabla|\mathbf{E}(\mathbf{r})|^2 \tag{8.1}$$

where ε_m is the permittivity of the medium surrounding the particle, R is the radius of the particle, ω is the radian frequency of the applied field, $\mathbf{r}$ refers to the vector spatial coordinate, and $\mathbf{E}$ is the applied vector electric field. The Clausius-Mossotti factor ($\underline{CM}$)—CM factor—gives the frequency (ω) dependence of the force, and its sign determines whether the particle experiences positive or negative DEP. Importantly, the above relation is limited to instances where the field is spatially invariant, in contrast to traveling-wave DEP or electrorotation (see [39, 45]).

Depending on the relative polarizabilities of the particle and the medium, the body will feel a force that propels it toward field maxima (termed positive DEP or p-DEP) or field minima (negative DEP or n-DEP). In addition, the direction of the force is independent of the polarity of the applied voltage; switching the polarity of the voltage does not change the direction of the force—it is still toward the field maximum in Figure 8.2. Thus DEP works equally well with both DC and AC fields.

DEP should be contrasted with electrophoresis, where one manipulates charged particles with electric fields [30], as there are several important differences. First, DEP does not require the particle to be charged in order to manipulate it; the particle must only differ electrically from the medium that it is in. Second, DEP works with AC fields, whereas no net electrophoretic movement occurs in such a field. Thus, with DEP one can use AC excitation to avoid problems such as electrode polarization effects [74] and electrolysis at electrodes. Even more importantly, the use of AC fields reduces membrane charging of biological cells, as explained below. Third, electrophoretic systems cannot create stable non-contact traps, as opposed to DEP—one needs electromagnetic fields to trap charges (electrophoresis can, though, be used to trap charges at electrodes [63]). Finally, DEP forces increase with the square of the electric field (described below), whereas electrophoretic forces increase linearly with the electric field.

This is not to say that electrophoresis is without applicability. It is excellent for transporting charged particles across large distances, which is difficult with DEP (though traveling-wave versions exist [17]). Second, many molecules are charged and are thus movable with this technique. Third, when coupled with electroosmosis, electrophoresis makes a powerful separation system, and has been used to great effect [30].

8.2.2.1. The Clausius-Mossotti Factor The properties of the particle and medium within which it resides are captured in the form of the Clausius-Mossotti factor (*CM*)—CM factor. The Clausius-Mossotti factor arises naturally during the course of solving Laplace's equation and matching the boundary conditions for the electric field at the surface of the particle (for example, see [45]). For a homogeneous spherical particle, the CM factor is given by

$$\underline{CM} = \frac{\underline{\varepsilon}_p - \underline{\varepsilon}_m}{\underline{\varepsilon}_p + 2\underline{\varepsilon}_m} \tag{8.2}$$

where $\underline{\varepsilon}_m$ and $\underline{\varepsilon}_p$ are the complex permittivities of the medium and the particle, respectively, and are each given by $\underline{\varepsilon} = \varepsilon + \sigma/(j\omega)$, where ε is the permittivity of the medium or particle, σ is the conductivity of the medium or particle, and j is $\sqrt{-1}$.

Many properties lie within this simple relation. First, one sees that competition between the medium ($\underline{\varepsilon}_m$) and particle ($\underline{\varepsilon}_p$) polarizabilities will determine the sign of CM factor, which will in turn determine the sign—and thus direction—of the DEP force. For instance, for purely dielectric particles in a non-conducting liquid ($\sigma_p = \sigma_m = 0$), the CM factor is purely real and will be positive if the particle has a higher permittivity than the medium, and negative otherwise.

Second, the real part of the CM factor can only vary between $+1$ ($\underline{\varepsilon}_p \gg \underline{\varepsilon}_m$, e.g., the particle is much *more* polarizable than the medium) and -0.5 ($\underline{\varepsilon}_p \ll \underline{\varepsilon}_m$, e.g., the particle is much *less* polarizable than the medium). Thus n-DEP can only be half as strong as p-DEP. Third, by taking the appropriate limits, one finds that at low frequency the CM factor (Eqn. (8.2)) reduces to

$$\underset{\omega\to 0}{CM} = \frac{\sigma_p - \sigma_m}{\sigma_p + 2\sigma_m} \tag{8.3}$$

while at high frequency it is

$$\underset{\omega\to \infty}{CM} = \frac{\varepsilon_p - \varepsilon_m}{\varepsilon_p + 2\varepsilon_m} \tag{8.4}$$

Thus, similar to many electroquasistatic systems, the CM factor will be dominated by relative permittivities at high frequency and conductivities at low frequencies; the induced dipole varies between a free charge dipole and a polarization dipole. The relaxation time separating the two regimes is

$$\tau_{MW} = \frac{\varepsilon_p + 2\varepsilon_m}{\sigma_p + 2\sigma_m} \tag{8.5}$$

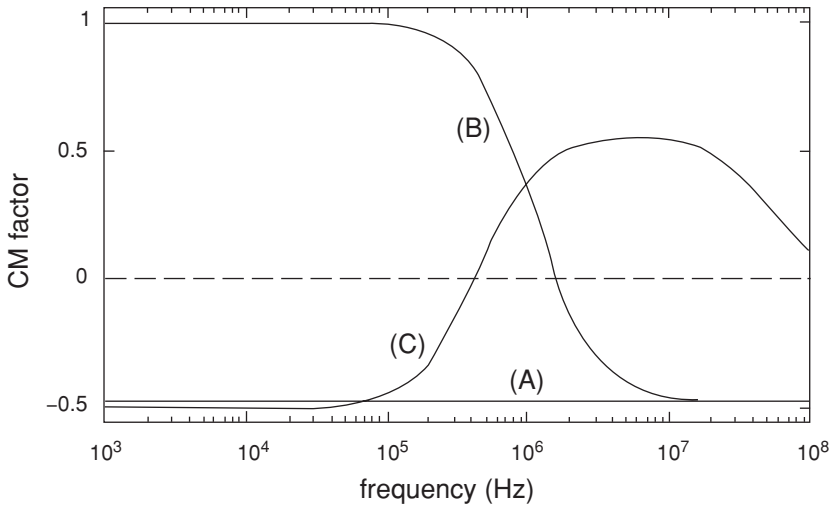

FIGURE 8.3. CM factor for three situations. **(A)** A non-conducting uniform sphere with $\varepsilon_p = 2.4$ in non-conducting water ($\varepsilon_m = 80$). The water is much more polarizable than the sphere, and thus the CM factor is ~ -0.5. (**B**) The same sphere, but with a conductivity $\sigma_p = 0.01$ S/m in non-conducting water. Now there is one dispersion—at low frequencies the bead is much more conducting than the water & hence there is p-DEP, while at high frequencies the situation is as in (A). (**C**) A spherical shell (approximating a mammalian cell), with ($\varepsilon_{cyto} = 75$, $c_m = 1$ μF/cm^2, $\sigma_{cyto} = 0.5$ S/m, $g_m = 5$ mS/cm^2) in a 0.1 S/m salt solution, calculated using results from [45]. Now there are two interfaces and thus two dispersions. Depending on the frequency, the shell can experience n-DEP or p-DEP.

and is denoted τ_{MW} to indicate that the physical origin is Maxwell-Wagner interfacial polarization [73].

This Maxwell-Wagner interfacial polarization causes the frequency variations in the CM factor. It is due to the competition between the charging processes in the particle and medium, resulting in charge buildup at the particle/medium interface. If the particle and medium are both non-conducting, then there is no charge buildup and the CM factor will be constant with no frequency dependence (Figure 8.3A). Adding conductivity to the system results in a frequency dispersion in the CM factor due to the differing rates of interfacial polarization at the sphere surface (Figure 8.3B).

While the uniform sphere model is a good approximation for plastic microspheres, it is possible to extend this expression to deal with more complicated particles such as biological cells, including non-spherical ones.

Multi-Shelled Particulate Models Because we are interested in creating traps that use DEP to manipulate cells, we need to understand the forces on cells in these systems. Luckily, the differences between a uniform sphere and a spherical cell can be completely encompassed in the CM factor; the task is to create an electrical model of the cell and then solve Laplace's equation to derive its CM factor (a good review of electrical properties of cells is found in Markx and Davey [57]). The process is straightforward, though tedious, and has been covered in detail elsewhere [39, 43, 45]. Essentially, one starts by adding a thin shell to the uniform sphere and matches boundary conditions at now two interfaces,

deriving a CM factor very similar to Eqn (8.2) but with an effective complex permittivity $\underline{\varepsilon}'_p$ that subsumes the effects of the complicated interior (see §5.3 of Hughes [39]). This process can be repeated multiple times to model general multi-shelled particles.

Membrane-Covered Spheres: Mammalian Cells, Protoplasts Adding a thin shell to a uniform sphere makes a decent electrical model for mammalian cells and protoplasts. The thin membrane represents the insulating cell membrane while the sphere represents the cytoplasm. The nucleus is not modeled is this approximation. For this model the effective complex permittivity can be represented by:

$$\underline{\varepsilon}'_p = \frac{\underline{c}_m R \cdot \underline{\varepsilon}_{cyto}}{\underline{c}_m R + \underline{\varepsilon}_{cyto}} \tag{8.6}$$

where $\underline{\varepsilon}_{cyto}$ is the complex permittivity of the cytoplasmic compartment and $\underline{c}_m$ refers to complex membrane capacitance per unit area and is given by

$$\underline{c}_m = c_m + g_m/(j\omega) \tag{8.7}$$

where c_m and g_m are the membrane capacitance and conductance per unit area (F/m^2 and S/m^2) and can be related to the membrane permittivity and conductivity by $c_m = \varepsilon_m/t$ and $g_m = \sigma_m/t$, where t is the membrane thickness. The membrane conductance of intact cells is often small and can be neglected. Because cell membranes are comprised of phospholipid bilayers whose thickness and permittivity varies little across cell types, the membrane capacitance per unit area is fairly fixed at $c_m \sim 0.5 - 1\mu F/cm^2$ [64].

Plotting a typical CM factor for a mammalian cell shows that it is more complicated than for a uniform sphere. Specifically, since it has two interfaces, there are two dispersions in its CM factor, as shown in Figure 8.3C. In low-conductivity buffers, the cell will experience a region of p-DEP, while in saline or cell-culture media the cells will only experience n-DEP. This last point has profound implications for trap design. If one wishes to use cells in physiological buffers, one is restricted to n-DEP excitation, irrespective of applied frequency. Only by moving low-conductivity solutions can one create p-DEP forces in cells. While, as we discuss below, p-DEP traps are often easier to implement, one must then deal with possible artifacts due to the artificial media.

One challenge for the designer in applying different models for the CM factor is getting accurate values for the different layers. In Table 8.1 we list properties culled from the literature for several types of particles, along with the appropriate literature references. Care must be taken in applying these, as some of the properties may be dependent on the cell type, cell physiology, and suspending medium, as well as limited by the method in which they were measured. Besides the values listed below, there are also values on Jurkat cells [67] and other white blood cells [21].

Sphere with Two Shells: Bacteria and Yeast Bacteria and yeast have a cell wall in addition to a cell membrane. Iterating on the multi-shell model can be used to derive a CM factor these types of particles [35, 76, 95]. Griffith *et al*. also used a double-shell model, this time to include the nucleus of a mammalian cells, in this case the human neutrophil [29].

TABLE 8.1. Parameters for the electrical models of different cells and for saline.

		Inner compartment		Membrane			Wall		
Particle type	Radius (μ m)	ε	σ (S/m)	ε	σ (S/m)	thickness (nm)	ε	σ(S/m)	thickess (nm)
Latex microspheres	nm–μ m	2.5	2e-4	—	—	—	—	—	—
Yeast [96, 97]	4.8	60	0.2	6	250e-9	8	60	0.014	∼200
E. coli [76]	1	60	0.1	10	50e-9	5	60	0.5	20
HSV-1 virus [40]	0.25	70	8e-3	10	$\sigma_p = 3.5$ nS		—	—	—
HL-60 [37]	6.25	75	0.75	1.6 μ F/cm^2	0.22 S/cm^2	1	—	—	—
PBS	—	78–80	1.5	—	—	—	—	—	—

Surface Conduction: Virus and Other Nanoparticles Models for smaller particles must also accommodate surface currents around the perimeter of the particle. As particles get smaller, this current path becomes more important and affects the CM factor (by affect the boundary conditions when solving Laplace's equation). In this case, the conductivity of the particle can be approximated by [39]

$$\sigma_p + \frac{2K_s}{R} \tag{8.8}$$

where K_s represents the surface conductivity (in Siemens). One sees that this augments the bulk conductivity of the particle (σ_p) with a surface-conductance term inversely proportional to the particle radius.

Non-Spherical Cells Many cells are not spherical, such as some bacteria (e.g., *E. coli*) and red blood cells. The CM factor can be extended to include these effects by introducing a depolarizing factor, described in detail in Jones' text [45].

8.2.2.2. Multipolar Effects The force expression given in Eqn (8.1) is the most commonly used expression for the DEP force applied to biological particles, and indeed accurately captures most relevant physics. However, it is not strictly complete, in that the force calculated using that expression assumes that only a dipole is induced in the particle. In fact, arbitrary multipoles can be induced in the particle, depending on the spatial variation of the field that it is immersed in. Specifically, the dipole approximation will become invalid when the field non-uniformities become great enough to induce significant higher-order multipoles in the particle. This can easily happen in microfabricated electrode arrays, where the size of the particle can become equal to characteristic field dimensions. In addition, in some electrode geometries there exists field nulls. Since the induced dipole is proportional to the electric field, the dipole approximation to the DEP force is zero there. Thus at least the quadrupole moment must be taken into account to correctly model the DEP forces in such configurations.

In the mid-90's Jones and Washizu extended their very successful effective-moment approach to calculate all the induced moments and the resultant forces on them [50, 51, 91, 92]. Gascoyne's group, meanwhile, used an approach involving the Maxwell's stress tensor to arrive at the same result [87]. Thus, it is now possible to calculate the DEP forces

in arbitrarily polarized non-uniform electric fields. A compact tensor representation of the final result in is

$$\mathbf{F}_{\mathbf{dep}}^{(n)} = \frac{\overline{\overline{\vdots}}^{\,(n)}[\cdot]^n(\nabla)^n\mathbf{E}}{n!} \tag{8.9}$$

where n refers to the force order ($n = 1$ is the dipole, $n = 2$ is the quadropole, etc.), $\overline{\overline{\vdots}}^{\,(n)}$ is the multipolar induced-moment tensor, and $[\cdot]^n$ and $(\nabla)^n$ represent n dot products and gradient operations. Thus one sees that the n-th force order is given by the interaction of the n-th-order multipolar moment with the n-th gradient of the electric field. For $n = 1$ the result reverts to the force on a dipole (Eqn (8.1)).

A more explicit version of this expression for the time-averaged force in the i-th direction (for sinusoidal excitation) is

$$\begin{aligned}
\left\langle F_i^{(1)} \right\rangle &= 2\pi\varepsilon_m R^3 Re\left[\underline{CM}^{(1)}\underline{E}_m\frac{\partial}{\partial x_m}\underline{E}_i^*\right] \\
\left\langle F_i^{(2)} \right\rangle &= \frac{2}{3}\pi\varepsilon_m R^5 Re\left[\underline{CM}^{(2)}\frac{\partial}{\partial x_m}\underline{E}_n\frac{\partial^2}{\partial x_n\partial x_m}\underline{E}_i^*\right] \\
&\vdots
\end{aligned} \tag{8.10}$$

for the dipole ($n = 1$) and quadrupole ($n = 2$) force orders [51]. The Einstein summation convention has been applied in Eqn. (8.10). While this approach may seem much more difficult to calculate than Eqn (8.1), compact algorithms have been developed for calculating arbitrary multiples [83]. The multipolar CM factor for a uniform lossy dielectric sphere is given by

$$\underline{CM}^{(n)} = \frac{\underline{\varepsilon}_p - \underline{\varepsilon}_m}{n\underline{\varepsilon}_p + (n+1)\underline{\varepsilon}_m} \tag{8.11}$$

It has the same form as the dipolar CM factor (Eqn. (2)) but has smaller limits. The quadrupolar CM factor ($n = 2$), for example, can only vary between $+1/2$ and $-1/3$.

8.2.2.3. Scaling Although the force on a dipole in a non-uniform field has been recognized for decades, the advent of microfabrication has really served as the launching point for DEP-based systems. With the force now defined, I will now investigate why downscaling has enabled these systems.

Most importantly, reducing the characteristic size of the system reduces the applied voltage needed to generate a given field gradient, and for a fixed voltage increases that field gradient. A recent article on scaling in DEP-based systems [46] illustrates many of the relevant scaling laws. Introducing the length scale L into Eqn (8.1) and appropriately approximating derivatives, one gets that the DEP force (dipole term) scales as

$$F_{dep} \sim R^3\frac{V^2}{L^3} \tag{8.12}$$

illustrating the dependency. This scaling law has two enabling implications. First, generating the forces required to manipulate micron-sized bioparticles (∼pN) requires either large voltages (100's–1000's V) for macroscopic systems (1–100 cm) or small voltages (1–10 V) for microscopic systems (1–100 μm). Large voltages are extremely impractical to generate at the frequencies required to avoid electrochemical effects (kHz–MHz). Slew rate limitations in existing instrumentation make it extremely difficult to generate more than 10 V_{pp} at frequencies above 1 MHz. Once voltages are decreased, however, one approaches the specifications of commercial single-chip video amplifiers, commodity products that can be purchased for a few dollars.

The other strong argument for scaling down is temperature. Biological systems can only withstand certain temperature excursions before their function is altered. Electric fields in conducting liquids will dissipate power, heating the liquid. Although even pure water has a finite conductivity (∼5 μS/m), the problem is more acute as the conductivity of the water increases. For example, electrolytes typically used to culture cells are extremely conductive (∼1 S/m). While the exact steady-state temperature rise is determined by the details of electrode geometry and operating characteristics, the temperature rise, as demonstrated by Jones [46], scales as

$$\Delta T \sim \sigma \cdot V^2 \cdot L^3 \tag{8.13}$$

where σ is the conductivity of the medium. It is extremely difficult to limit these rises by using convective heat transfer (e.g., flowing the media at a high rate); in these microsystems conduction is the dominant heat-transfer mechanism unless the flowrate is dramatically increased. Thus, one sees the strong ($\sim L^3$) argument for scaling down; it can enable operation in physiological buffers without significant concomitant temperature rises.

Temperature rise has other consequences besides directly affecting cell physiology. The non-uniform temperature distribution creates gradients in the electrical properties of the medium (because permittivity and conductivity are temperature-dependent). These gradients in turn lead to free charge in the system, which, when acted upon by the electric field, drag fluid and create (usually) destabilizing fluid flows. These electrothermal effects are covered in §2.3.3.

Thus, creating large forces is limited by either the voltages that one can generate or the temperature rises (and gradients) that one creates, and is always enhanced by decreasing the characteristic length of the system. All of these factors point to microfabrication as an enabling fabrication technology for DEP-based systems.

8.2.3. Other Forces

DEP interacts with other forces to produce a particle trap. The forces can either be destabilizing (e.g., fluid drag, gravity) or stabilizing (e.g., gravity).

8.2.3.1. Gravity The magnitude of the gravitational force is given by

$$F_{grav} = \frac{4}{3}\pi R^3(\rho_p - \rho_m)g \tag{8.14}$$

where ρ_m and ρ_p refer to the densities of the medium and the particle, respectively, and g is the gravitational acceleration constant. Cells and beads are denser than the aqueous media and thus have a net downward force.

8.2.3.2. Hydrodynamic Drag Forces Fluid flow past an object creates a drag force on that object. In most systems, this drag force is the predominant destabilizing force. The fluid flow can be intentional, such as that created by pumping liquid past a trap, or unintentional, such as electrothermal flows.

The universal scaling parameter in fluid flow is the Reynolds number, which gives an indication of the relative strengths of inertial forces to viscous forces in the fluid. At the small length scales found in microfluidics, viscosity dominates and liquid flow is laminar. A further approximation assumes that inertia is negligible, simplifying the Navier-Stokes equations even further into a linear form. This flow regime is called creeping flow or Stokes flow and is the common approximation taken for liquid microfluidic flows.

In creeping flow, a sphere in a uniform flow field will experience a drag force—called the Stokes' drag—with magnitude

$$F_{drag} = 6\pi\eta R v \tag{8.15}$$

where η is the viscosity of the liquid and v is the far-field relative velocity of the liquid with respect to the sphere. As an example, a 1-μm-diameter particle in a 1-mm/s water flow will experience ~10 pN of drag force.

Unfortunately, it is difficult to create a uniform flow field, and thus one must broaden the drag force expression to include typically encountered flows. The most common flow pattern in microfluidics is the flow in a rectangular channel. When the channel is much wider than it is high, this flow can be approximated as the one-dimensional flow between to parallel plates, or plane Poiseuille flow. This flow profile is characterized by a parabolic velocity distribution where the centerline velocity is 1.5× the average linear flow velocity

$$v(z) = 1.5\frac{Q}{wh}\left(1 - \left(\frac{z - h/2}{h/2}\right)^2\right) \tag{8.16}$$

where Q is the volume flowrate, w and h are the width and height of the channel, respectively, and z is the height above the substrate at which the velocity is evaluated. The expression in Eqn (8.15) can then be refined by using the fluid velocity at the height of the particle center.

Close to the channel wall ($z \ll h$) the quadratic term in Eqn (8.16) can be linearly approximated, resulting a velocity profile known as plane shear or plane Couette flow

$$v(z) = 1.5\frac{Q}{wh}\left(4\frac{z}{h}\right) = 6\frac{Q}{wh}\frac{z}{h} \tag{8.17}$$

The error between the two flow profiles increases linearly with z for $z \ll h/2$; the error when $z = 0.1 \cdot h$ is ~10%.

Using Eqn (8.15) with the modified fluid velocities is a sufficient approximation for the drag force in many applications, and is especially useful in non-analytical flow profiles

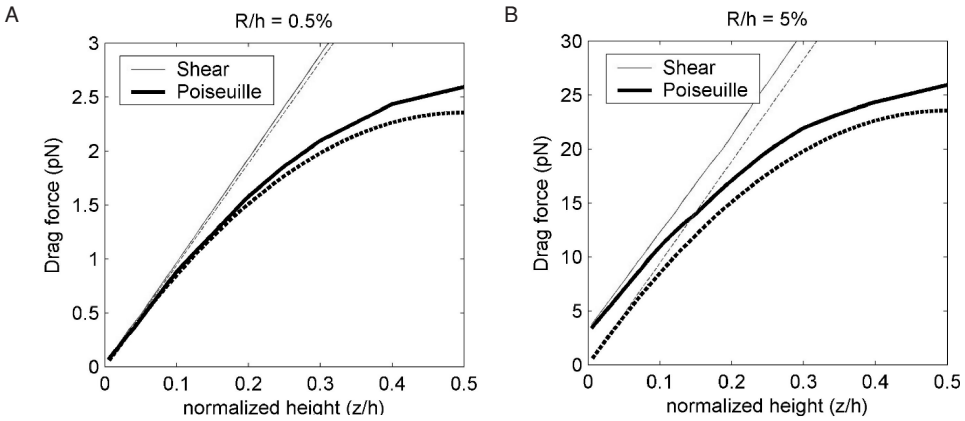

FIGURE 8.4. Drag force using different approximations for a particle that is 0.5% (**A**) and 5% (**B**) of the chamber height. For the smaller particle (A), all approaches give the same result near the surface. For larger particles (B), the exact formulations (—) give better results than approximate approaches (- - -).

derived by numerical modeling. In that case one can compute the Stokes' drag at each point by multiplying Eqn. (8.15) with the computed 3-D velocity field. To get a more exact result, especially for particles that are near walls, one can turn to solved examples in the fluid mechanics literature. Of special interest to trapping particles, the drag force on both a stationary and moving sphere near a wall in both plane Poiseuille [19] and shear flow [26] has been solved. The calculated drag forces have the same form as Eqn (8.15) but include a non-dimensional multiplying factor that accounts for the presence of the wall.

In Figure 8.4 I compare drag forces on 1 μm and 10 μm-diameter spheres using the different formulations. In both cases, the channel height is fixed at 100 μm. One sees two very different behaviors. When the sphere size is small compared to the channel height ($R = 0.5\%$ of h), all four formulations give similar results near the chamber wall (Figure 8.4A), with the anticipated divergence of the shear and Poiseuille drag profiles away from the wall. However, as the sphere becomes larger compared to the chamber height (Figure 8.4B), the different formulations diverge. Both the shear and parabolic profiles calculated using a single approach converge to identical values at the wall, but the two approaches yield distinctly different results. In this regime the drag force calculated using Eqn. (8.15) consistently underestimates the drag force, in this case by about 2 pN. This has a profound effect near the wall, where the actual drag force is 50% higher than that estimated by the simple approximation. Thus, for small particles ($R \ll h$) away from walls ($z \gg R$), the simple approximation is fine to within better than 10%, while in other cases one should use the exact formulations.

While spheres approximate most unattached mammalian cells as well as yeast and many bacteria, other cells (e.g., *E. coli,* erythrocytes) are aspherical. For these particles, drag forces have the same form as Eqn. (8.15) except that term $6\pi\eta R$ is replaced by different "friction" factors, nicely catalogued by Morgan and Green [60].

8.2.3.3. Electrothermal Forces The spatially non-uniform temperature distribution created by the power dissipated by the electric field can lead to flows induced by

electrothermal effects. These effects are covered in great detail by Morgan and Green [60]. Briefly, because the medium permittivity and conductivity are functions of temperature, temperature gradients directly lead to gradients in ε and σ. These gradients in turn generate free charge which can be acted upon by an electric field to move and drag fluid along with it, creating fluid flow. This fluid flow creates a drag force on an immersed body just as it does for conventional Stokes' drag (Eqn. (8.15)). In general, derivations of the electrothermal force density, the resulting liquid flow, and the drag require numerical modeling because the details of the geometry profoundly impact the results. Castellanos *et al.* have derived solutions for one simple geometry, and have used it to great effect to derive some scaling laws [6].

8.3. DESIGN FOR USE WITH CELLS

Since dielectrophoretic cell manipulation exposes cells to strong electric fields, one needs to know how these electric fields might affect cell physiology. Ideally, one would like to determine the conditions under which the trapping will not affect the cells and use those conditions to constrain the design. Of course, cells are poorly understood complex systems and thus it is impossible to know for certain that one is not perturbing the cell. However, all biological manipulations—cell culture, microscopy, flow cytometer, etc.—alter cell physiology. What's most important is to minimize known influences on cell behavior and then use proper controls to account for the unknown influences. In short, good experimental design.

The known influences of electric fields on cells can be split into the effects due to current flow, which causes heating, and direct interactions of the fields with the cell. We'll consider each of these in turn.

Au: Pls. check Headings Number.

8.3.1.1. Current-Induced Heating Electric fields in a conductive medium will cause power dissipation in the form of Joule heating. The induced temperature changes can have many effects on cell physiology. As mentioned previously, microscale DEP is advantageous in that it minimizes temperature rises due to dissipated power. However, because cells can be very sensitive to temperature changes, it is not assured that any temperature rises will be inconsequential.

Temperature is a potent affecter of cell physiology [4, 11, 55, 75]. Very high temperatures ($>4\,^{\circ}$C above physiological) are known to lead to rapid mammalian cell death, and research has focused on determining how to use such knowledge to selectively kill cancer cells [81]. Less-extreme temperature excursions also have physiological effects, possibly due to the exponential temperature dependence of kinetic processes in the cell [93]. One well-studied response is the induction of the heat-shock proteins [4, 5]. These proteins are molecular chaperones, one of their roles being to prevent other proteins from denaturing when under environmental stresses.

While it is still unclear as to the minimum temperature excursion needed to induce responses in the cell, one must try to minimize any such excursions. A common rule of thumb for mammalian cells is to keep variations to $<1\,^{\circ}$C, which is the approximate daily variation in body temperature [93]. The best way we have found to do this is to numerically solve for the steady-state temperature rise in the system due to the local heat sources given

by σE^2. Convection and radiation can usually be ignored, and thus the problem reduces to solving for the conduction heat flow subject to the correct boundary conditions. Then, using the scaling of temperature rise with electric field and fluid conductivity (Eqn. (8.13)), one can perform a parametric design to limit temperature rises.

8.3.1.2. Direct Electric-Field Interactions Electric fields can also directly affect the cells. The simple membrane-covered sphere model for mammalian cells can be used to determine where the fields exist in the cell as the frequency is varied. From this one can determine likely pathways by which the fields could impact physiology [31, 73]. Performing the analysis indicates that the imposed fields can exist across the cell membrane or the cytoplasm. A qualitative electrical model of the cell views the membrane as a parallel RC circuit connected in-between RC pairs for the cytoplasm and the media. At low frequencies (<MHz) the circuit looks like three resistors in series and because the membrane resistance is large the voltage is primarily dropped across it. This voltage is distinct from the endogenous transmembrane potential that exists in the cell. Rather, it represents the voltage derived from the externally applied field. The total potential difference across the cell membrane would be given by the sum of the imposed and endogenous potentials. At higher frequencies the impedance of the membrane capacitor decreases sufficiently that the voltage across the membrane starts to decrease. Finally, at very high frequencies (100's MHz) the model looks like three capacitors in series and the membrane voltage saturates.

Quantitatively, the imposed transmembrane voltage can be derived as [73]

$$|V_{tm}| = \frac{1.5|\mathbf{E}|R}{\sqrt{1+(\omega\tau)^2}} \tag{8.18}$$

where ω is the radian frequency of the applied field and τ is the time constant given by

$$\tau = \frac{Rc_m(\rho_{cyto} + 1/2\rho_{med})}{1 + Rg_m(\rho_{cyto} + 1/2\rho_{med})} \tag{8.19}$$

where ρ_{cyto} and ρ_{med} med are the cytoplasmic and medium resistivities (Ω-m). At low frequencies $|V_m|$ is constant at $1.5|\mathbf{E}|$R but decreases above the characteristic frequency $(1/\tau)$. This model does not take into account the high-frequency saturation of the voltage, when the equivalent circuit is a capacitive divider.

At the frequencies used in DEP—10's kHz to 10's MHz—the most probably route of interaction between the electric fields and the cell is at the membrane [79]. There are several reasons for this. First, electric fields already exist at the cell membrane, leading to transmembrane voltages in the 10's of millivolts. Changes in these voltages could affect voltage-sensitive proteins, such as voltage-gated ion channels [7]. Second, the electric field across the membrane is greatly amplified over that in solution. From Eqn. (6.18) one gets that at low frequencies

$$\begin{aligned} |V_{tm}| &= \frac{1.5|\mathbf{E}|R}{\sqrt{1+(\omega\tau)^2}} \approx 1.5|\mathbf{E}|R \\ |E_{tm}| &\approx |V_m|/t = (1.5R/t)\cdot|\mathbf{E}| \end{aligned} \tag{8.20}$$

and thus at the membrane the imposed field is multiplied by a factor of 1.5 R/t ($\sim$1000), which can lead to quite large membrane fields (E_{tm}). This does not preclude effects due to cytoplasmic electric fields. However, these effects have not been as intensily studied, perhaps because 1) those fields will induce current flow and thus heating, which is not a direct interaction, 2) the fields are not localized to an area (e.g., the membrane) that is likely to have field-dependent proteins, and 3) unlike the membrane fields, the cytoplasmic fields are not amplified.

Several studies have investigated possible direct links between electric fields and cells. At low frequencies, much investigation has focused on 60-Hz electromagnetic fields and their possible effects, although the studies thus far are inconclusive [54]. DC fields have also been investigated, and have been shown to affect cell growth [44] as well as reorganization of membrane components [68]. At high frequencies, research has focused on the biological effects of microwave radiation, again inconclusively [65].

In the frequency ranges involved in DEP, there has been much less research. Tsong has provided evidence that some membrane-bound ATPases respond to fields in the kHz–MHz range, providing at least one avenue for interaction [79]. Electroporation and electrofusion are other obvious, although more violent, electric field-membrane coupling mechanisms [98].

Still other research has been concerned specifically with the effects of DEP on cells, and has investigated several different indicators of cell physiology to try to elucidate any effects. One of the first studies was by the Fuhr et al., who investigated viability, anchorage time, motility, cell growth rates, and lag times after subjecting L929 and 3T3 fibroblast cells in saline to short and long (up to 3 days) exposure to 30–60 kV/m fields at 10–40 MHz near planar quadrupoles [16]. They estimated that the transmembrane load was $<$20 mV. The fields had no discernable effect.

Another study investigated changes in cell growth rate, glucose uptake, lactate and monoclonal antibody production in CHO & HFN 7.1 cells on top of interdigitated electrodes excited at 10 MHz with $\sim 10^5$ V/m in DMEM (for the HFN 7.1 cells) or serum-free medium (for the CHO cells) [12]. Under these conditions they observed no differences in the measured properties between the cells and control populations.

Glasser and Fuhr attempted to differentiate between heating and electric-field effects on L929 mouse fibroblast cells in RPMI to the fields from planar quadrupoles [24]. They imposed $\sim$40 kV/m fields of between 100 kHZ and 15 MHz for 3 days and observed monolayers of cells near the electrodes with a video microscopy setup, similar to their previous study [16]. They indirectly determined that fields of $\sim$40 kV/m caused an $\sim 2\,^{\circ}$C temperature increase in the cells, but did not affect cell-division rates. They found that as they increased field frequency (from 500 kHZ to 15 MHz) the maximum tolerable field strength (before cell-division rates were altered) increased. This is consistent with a decrease in the transmembrane load with increasing frequency.

Wang et al. studied DS19 murine erythroleukemia cells exposed to fields ($\sim 10^5$ V/m) of 1 kHz–10 MHz in low-conductivity solutions for up to 40-min [90]. They found no effects due to fields above 10 kHz. They determined that hydrogen peroxide produced by reactions at the electrode interfaces for 1 kHz fields caused changes in cell growth lag phase, and that removal of the peroxide restored normal cell growth.

On the p-DEP side, Archer et al. subjected fibroblast-like BHK 21 C13 cells to p-DEP forces produced by planar electrodes arranged in a sawtooth configuration [1]. They used low-conductivity (10 mS/m) isoosmotic solutions and applied fields of $\sim 10^5$ V/m at 5 MHz. They monitored cell morphology, cell doubling time, oxidative respiration (mitochondrial stress assay), alterations in expression of the immediate-early protein fos, and non-specific gene transcription directly after a 15 minute exposure and after a 30-min time delay. They observed 20–30% upregulation of fos expression and a upregulation of a few unknown genes (determined via mRNA analysis). Measured steady-state temperatures near the cells were $<1\,^{\circ}$C above normal, and their calculated transmembrane voltage under their conditions was $<100\,\mu$V, which should be easily tolerable. The mechanism—thermal or electrical—of the increased gene expression was left unclear. It is possible that artifacts from p-DEP attraction of the cells to the electrodes led to observed changes. Either way, this study certainly demonstrates the possibility that DEP forces could affect cell physiology.

Finally, Gray *et al.* exposed bovine endothelial cells in sucrose media (with serum) to different voltages—and thus fields—for 30-min in order to trap them and allow them to adhere to their substrates. They measured viability and growth of the trapped cells and found that cell behavior was the same as controls for the small voltages but that large voltages caused significant cell death [27]. This study thus demonstrates the p-DEP operation in artificial media *under the proper conditions* does not grossly affect cell physiology.

In summary, studies specifically interested in the effects of kHz–MHz electroquasistatic fields on cells thus far demonstrate that choosing conditions under which the transmembrane loads and cell heating are small—e.g., >MHz frequencies, and fields in $\sim$10's kV/m range—can obviate any gross effects. Subtler effects, such as upregulation of certain genetic pathways or activation of membrane-bound components could still occur, and thus DEP, as with any other assay technique, must be used with care.

8.4. TRAP GEOMETRIES

The electric field, which creates the DEP force, is in turn created by electrodes. In this section I will examine some of the electrode structures used in this field and their applicability to trapping cells and other microparticles. The reader is also encouraged to read the relevant chapters in Hughes' [39] and Morgan and Green's texts [60], which contain descriptions of some field geometries.

One can create traps using either p-DEP or n-DEP. Using n-DEP a zero-force point is created away from electrodes at a field minimum and the particle is trapped by pushing at it from all sides. In p-DEP the zero-force point is at a field maximum, typically at the electrode surface or at field constrictions. Both approaches have distinct advantages and disadvantages, as outlined in Table 8.2. For each application, the designer must balance these to select the best approach.

8.4.1. n-DEP Trap Geometries

Although an infinite variety of electrode geometries can be created, the majority of research has focused on those that are easily modeled or easily created.

TABLE 8.2. Comparison of advantages and disadvantages of p-DEP and n-DEP approaches to trapping cells.

p-DEP	n-DEP
Must use low conductivity *artificial* media (−)	Can use saline or other high-salt buffers (+)
CM factor can go to +1 (+)	CM factor can go to −0.5 (−)
Less heating (+)	More heating (−)
Typically easier to trap by pulling (+)	Typically harder to trap by pushing (−)
Traps usually get stronger as V increases (+)	Traps often do not get stronger with increasing V (−)
Cells stick to or can be damaged by electrodes (−)	Cells are physically removed from electrodes (+)
Cells go to maximum electric field (−)	Cells go to minimum electric field (+)

8.4.1.1. Interdigitated Electrodes Numerous approximate and exact analytical solutions exist for the interdigitated electrode geometry (Figure 8.5A), using techniques as varied as conformal mapping [23, 82], Green's function [10, 86], and Fourier series [33, 61]. Recently, an elegant exact closed-form solution was derived [8]. Numerical solutions are also plentiful [28].

While the interdigitated electrode geometry has found much use in DEP separations, it does not make a good trap for a few reasons. First, the long extent of the electrodes in one direction creates an essentially 2-D field geometry and thus no trapping is possible along the length of the electrodes. Further, the spatial variations in the electric field—which create the DEP force—decrease exponentially away from the electrode surface. After about one electrode's worth of distance away from the susbtrate, the field is mostly uniform at a given height, and thus DEP trapping against fluid flows or other perpendicular forces cannot occur. Increasing the field to attempt to circumvent this only pushes the particle farther away from the electrodes, a self-defeating strategy; like the planar quadrupole [83], this trap is actually strongest at lower voltages, when the particle is on the substrate.

8.4.1.2. Quadrupole Electrodes Quadrupole electrodes are four electrodes with alternating voltage polarities applied to every other electrode (Figure 8.5B). The field for four point charges can be easily calculated by superposition, but relating the charge to voltage (via the capacitance) is difficult in general and must be done numerically.

Planar quadrupoles can create rudimentary particle traps (Figure 8.5B), and can trap single particles down to 100's of nm [40]. Using n-DEP, they provide in-plane particle confinement, and can provide three-dimensional confinement if the particle is denser than the suspending medium. As with interdigitated electrodes, however, these traps suffer from the drawback that increasing the field only pushes the particle farther out of the trap and does not necessarily increase confinement. We showed this in 2001 with measurements of the strength of these traps [83]. Unexpectedly, the traps are strongest at an intermediate voltage, just before the particle is about to be levitated (Figure 8.6).

A variant of the quadrupole electrodes is the polynomial electrode geometry (Figure 8.5C), introduced by Huang and Pethig in 1991 [36]. By placing the electrode edges at the equipotentials of the applied field, it is possible to analytically specify the field between the electrodes. One caveat of this approach is that it solves the 2-D Laplace equation, which is not strictly correct for the actual 3-D geometry; thus, the electric field is at best only truly specified right at the electrode surface, and not in all of space.

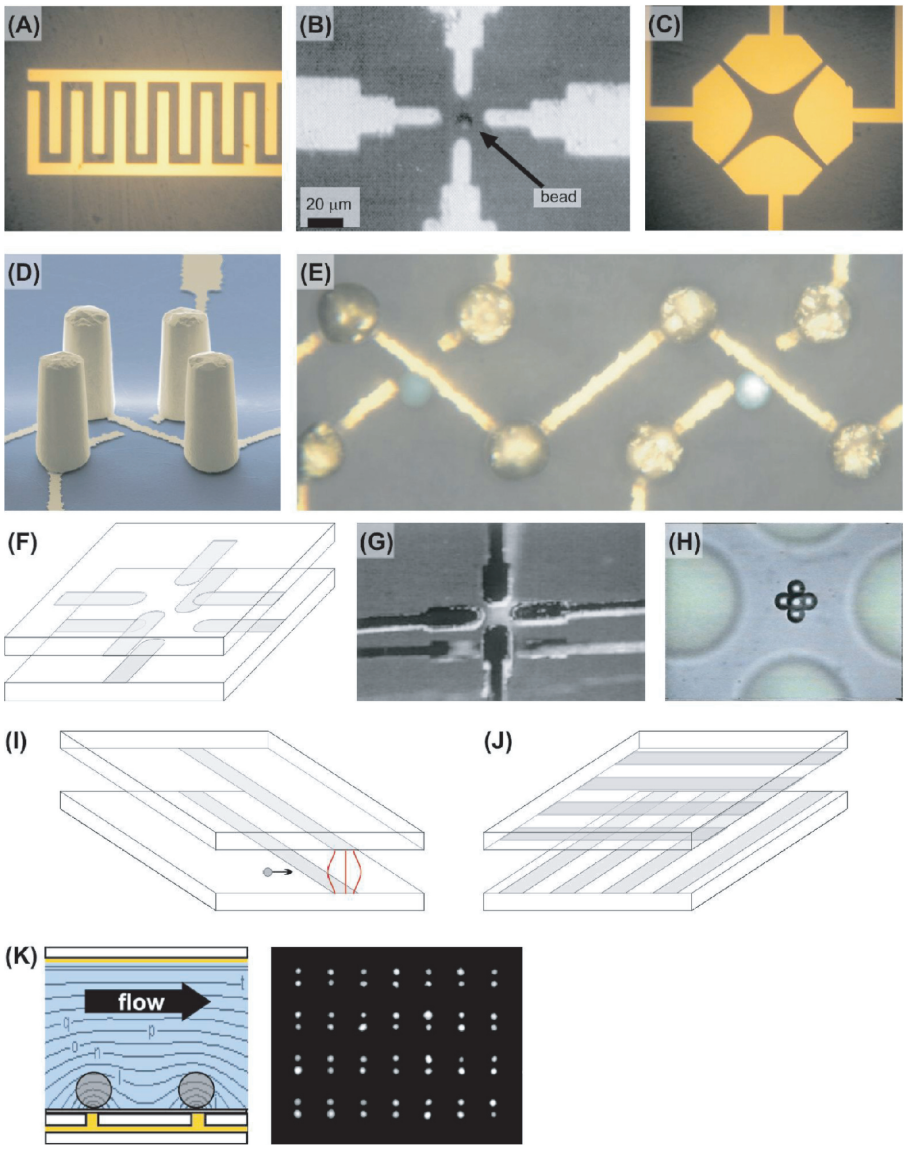

FIGURE 8.5. DEP trapping structures. **(A)** Interdigitated electrodes. **(B)** A planar quadrupole, showing a bead in the center. **(C)** Quadrupolar polynomial electrodes. **(D)** A 3-D view of an extruded quadrupole trap, showing the four gold post electrode electrodes and the gold wiring on the substrate. **(E)** A top-down image of two extruded quadrupole traps showing living trapped HL-60 cells in liquid. **(F–H)** Schematic (F), stereo image (G), and top-down view (H) of the oppose ocotpole, showing beads trapped at the center. **(I)** Schematic of the strip electrodes, showing the non-uniform electric field between them that creates an n-DEP force wall to incoming particles. **(J)** Schematic of the crossed-electrode p-DEP structure of Suehiro and Pethig [77]. **(K)** Side view schematic of Gray *et al.*'s p-DEP trap, showing the bottom point electrodes and the top plate, along with a top-down image of endothelial cells positioned at an array of traps.

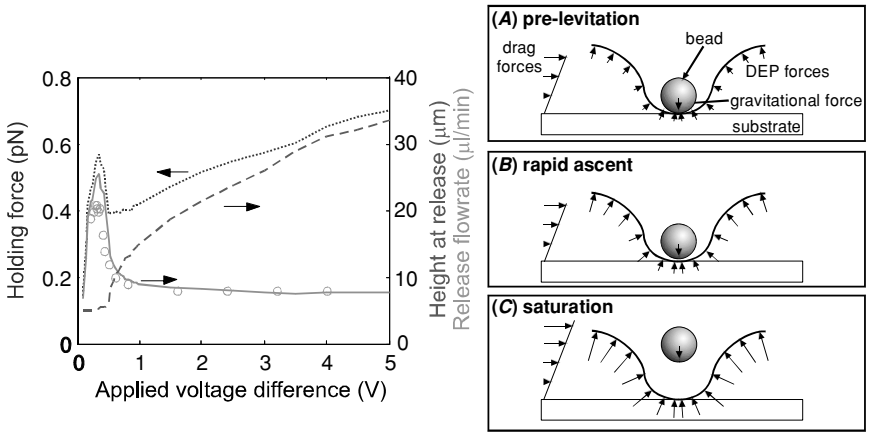

FIGURE 8.6. Behavior of planar quadrupole trap at different voltages, showing the measured (o) and simulated (—) release flowrate, the holding force (· · ·), and the height of the particle when it is released (- - -). (*A*) Pre-levitation. At very low voltages, the *z*-directed DEP force cannot overcome the gravitation force, and the bead is not levitated; (*B*) Rapid ascent. At a certain voltage the bead will just become levitated and the holding characteristics will peak; (*C*) Saturation. At high voltages, the increase in holding force is balanced by the increased particle levitation height, resulting in a flat release flowrate profile.

One way to avoid this behavior is to extend the electrodes into the third-dimension, creating extruded quadrupole traps (Figure 8.5D–E, [84, 85]). These traps, while much more difficult to make, are orders of magnitude stronger than the planar quadrupole traps, and can successfully hold single cells against significant liquid flows. These electrode geometries are sufficiently complicated that only numerical simulation can derive the correct field solution.

8.4.1.3. Octopole Electrodes Another way to increase the strength of quadrupole electrode traps is to put another quadrupole on the chamber ceiling to provide further particle confinement (Figure 8.5F–H). These opposed octopole traps are significantly stronger than planar quadrupoles, and are routinely used for single-particle trapping [69, 71]. They are much simpler to fabricate than the extruded quadrupoles, but are more complex to align and package.

8.4.1.4. Strip Electrodes Strip electrodes are simply two electrodes opposed from one-another, with one on the substrate and one on the chamber ceiling (Figure 8.5I). Introduced by Fiedler *et al.* in 1998, these have been used to create n-DEP "barriers" to herd particles [14]. The solution to this geometry has been analytically solved using conformal mapping [72]. As with the interdigitated electrodes, strip electrodes are of limited use for particle trapping because they only provide one dimension of confinement.

8.4.1.5. Other Electrode Structures Several other microscale trapping structures have been introduced. Some, like the castellated electrodes [22, 59] or round electrodes [34], which have been successfully used for particle separation, are not well-suited for trapping particles because of their planar format; they suffer the same drawbacks as the interdigitated and planar quadrupoles.

Recently, a team in Europe has been developing an active n-DEP-based trapping array [56]. Essentially, their device consists of a two-dimensional array of square electrodes and a conductive lid. The key is that incorporating CMOS logic (analog switches and memory) allows each square electrode to be connected to in-phase or out-of-phase AC voltage in a programmable fashion. By putting a center square at $+$V and the surrounding squares at $-$V, they can create an in-plane trap. Further putting the chamber top at $+$V closes the cage, giving 3-D confinement. The incorporation of CMOS further means that very few leads are required to control an indefinite number of sites, creating a readily scalable technology. Using this trap geometry, they have successfully manipulated both beads and cells, although moving cells from one site to another is currently quite slow ($\sim$sec).

8.4.2. p-DEP Trap Geometries

p-DEP traps, while easier to create, have seen less use, probably because the required low-conductivity media can perturb cell physiology (at least for mammalian cells) and because of concerns about electrode-cell interactions. As stated earlier, obtaining p-DEP with mammalian cells requires low-conductivity buffer, and this can create biological artifacts in the system. Nonetheless, several geometries do exist.

An early p-DEP-based trapping system was described by Suehiro and Pethig (Figure 8.5J, [77]). This used a set of parallel individually addressable electrodes on one substrate and another set of electrodes on the bottom substrate that were rotated 90°. By actuating one electrode on top and bottom, they could create a localized field maximum that could be moved around, allowing cell manipulation.

Another example is a concentric ring levitator that uses feedback-controlled p-DEP to actually trap particles away from electrodes [66]. In an air environment, they can levitate drops of water containing cells by pulling up against gravity with an upper electrode, feeding back the vertical position of the droplet to maintain a constant height.

Recently Gray *et al.* created a geometry consisting of a uniform top plate and electrode points on the substrate to create the field concentrations (Figure 8.5K, [27]). They were able to pattern cells onto the stubs using p-DEP. Importantly, experiments showed that the low-conductivity buffer did not affect the gross physiology of the cells at reasonable voltages. Finally, Chou *et al.* used geometric constrictions in an insulator to create field maxima in a conductivity-dominated system [9]. These maxima were used to trap DNA.

8.4.3. Lessons for DEP Trap Design

The preceding discussion raises some important points for DEP trap design. First, the choice of whether to trap via p-DEP or n-DEP is a system-level partitioning problem. For instance, if one absolutely requires use in saline, then n-DEP must be used. If, however, minimizing temperature rises is most important, then p-DEP may be better, as the low-conductivity media will reduce temperature rises. The decision may also be affected by fabrication facilities, etc.

In general, p-DEP traps are easier to create than n-DEP traps, because it is easier to hold onto a particle by attracting it than repelling it. The tradeoff is that p-DEP requires artificial media for use with mammalian cells. Nonetheless, the key for effective p-DEP is the creation of isolated field maxima. Because the particles are pulled into the field, p-DEP traps always trap stronger at higher voltages.

Creating effective n-DEP traps is more difficult, and requires some sort of three-dimensional confinement. This is difficult (though not impossible) to do with planar electrode structures, because the +z-component of the DEP force scales with voltage just as much as the in-plane components. This fundamentally pushes the particle away from the trap when one increases the voltage, drastically limiting trap strength. Any planar electrode structure, including the planar quadrupoles and interdigitated electrodes described above fail this test and therefore make a poor n-DEP trap. The two extant structures that exhibit strong trapping create three-dimensional trapping by removing the net +z-directed DEP force. Both the extruded quadrupole and opposed octopole structures do this by creating a structure that cancels out z-directed DEP forces at the trap center, enabling one to increase voltage—and thus trap strength—without pushing the particle farther away.

8.5. QUANTITATING TRAP CHARACTERISTICS

In order to assess whether a quantitative design is successful, one needs some quantitative validation of the fields and forces in DEP traps. Given that the complete DEP theory is known and that the properties of at least some particles are known, it should be possible to quantitate trap parameters. Those that are of interest include trap strength, field strength, and the spatial extents of the trap.

Measuring traps requires a quantitative readout. This typically takes the form of a test particle (or particles), whose location or motion can be measured and then matched against some prediction. Quantitative matching gives confidence in the validity of a particular modeling technique, thus allowing predictive design of new traps.

Starting in the 1970's, Tom Jones and colleagues explored DEP levitation in macroscopic electrode systems [47–49, 53]. Using both stable n-DEP traps and p-DEP traps with feedback control, they could measure levitation heights of different particles under various conditions. Knowledge of the gravitation force on the particle could then be used to as a probe of the equally opposing DEP forces at equilibrium.

Levitation measurements have continued to the present day, but now applied to microfabricated electrode structures, such as levitation height measurements of beads in planar quadrupoles [15, 25, 32], or on top of interdigitated electrodes [37, 58]. In all these measurements, errors arise because of the finite depth of focus of the microscope objective and because it is difficult to consistently focus on the center of the particle. The boundary between levitation and the particle sitting on the ground is a "sharp" event and is usually easier to measure and correlate to predictions than absolute particle height [25].

Wonderful pioneering work in quantitating the shapes of the fields was reported by the group in Germany in the 1992 and 1993 when they introduced their planar quadrupole [15] and opposed octopole [69] trap geometries. In the latter paper, the authors trapped 10's of beads that were much smaller than the trap size. The beads packed themselves to minimize their overall energy, in the process creating surfaces that reflected the force distribution in the trap. By comparing the experimental and predicted surfaces, they could validate their modeling.

An early velocity-measurement approach was described X.-B. Wang *et al.*, who used spiral electrodes and measured radial velocity and levitation height of breast cancer cells as they varied frequency, particle radius, and medium conductivity [89]. They then matched

the data to DEP theory, using fitting parameters to account for unknown material properties, and obtained good agreement. These researchers performed similar analyses using erythroleukemia cells in interdigitated electrode geometries, again obtaining good fits of the data to the theory [88].

Another approach that compares drag force to DEP force is described by Tsukahara *et al.*, where they measured the velocity as a particle moved toward or away from the minimum in a planar quadrupole polynomial electrode [80]. If the electric field and particle properties are known, it should be possible to relate the measured velocity to predictions, although, as described earlier, the use of Stokes drag introduces errors when the particle is near the wall and the forces they calculated for their polynomial electrodes are only valid at the electrode symmetry plane. This was reflected in the use of a fitting parameter to match predictions with experiment, although in principle absolute prediction should be possible.

The German team that initially introduced the idea of opposed electrodes on both the bottom and top of the chamber have continued their explorations into this geometry with great success. They have attempted to quantify the strength of their traps in two different ways. In the first approach, they measure the maximum flowrate against which a trap can hold a particle. Because of the symmetry of their traps, the particles are always along the midline of the flow, and by approximating the drag force on the particle with the Stokes drag (Eqn (8.15)) they can measure the strength of the trap in piconewtons [13, 62, 72]. Because they can calculate the electric fields and thus DEP forces, they have even been able to absolutely correlate predictions to experiment [72]. With such measurements they have determined that their opposed electrode devices can generate $\sim$20pN of force on 14.9-μm diameter beads [62].

The other approach that these researchers have taken to measuring trap strength is to combine DEP octopole traps with optical tweezers [2]. If the strength of one of the trapping techniques is known then it can be used to calibrate the other. In one approach, this was done by using optical tweezers to displace a bead from equilibrium in a DEP trap, then measuring the voltage needed to make that bead move back to center [18]. They used this approach to measure the strength of the optical tweezers by determining the DEP force on the particle at that position at the escape voltage. In principle, one could use this to calibrate the trap if the optical tweezer force constant was known.

In the other approach, at a given voltage and optical power, they measured the maximum that the bead could be displaced from the DEP minimum before springing back [70]. This is very similar to the prior approach, although it also allows one to generate a force-displacement characteristic for the DEP trap, mapping out the potential energy well.

A clever and conceptually similar approach was tried by Hughes and Morgan with a planar quadrupole [41], although in this case the unknown was the thrust exerted by *E. coli* bacteria. By measuring the maximum point that the bacteria could be displaced from the DEP trap minimum, they could back out the bacterial thrust if the DEP force characteristic in the trap was known. They achieved good agreement between predictions and modeling, at least at lower voltages.

For much smaller particles, where statistics are important, Chou *et al*. captured DNA in electrodeless p-DEP traps. They used the spatial distribution of the bacteria to measure the strength of the traps [9]. They measured the width of the fluorescence intensity distribution of labeled DNA in the trap, and assuming that the fluorescence intensity was linearly related to concentration, could extract the force of the trap by equating the "Brownian" diffusive

force to the DEP force. The only unknown in this approach, besides the assumptions of linearity, was the temperature, which could easily be measured.

In our lab we have been interested in novel trap geometries to enable novel trapping functionalities. One significant aim has been to create DEP traps for single cells that are strong enough to hold against significant liquid flows, such that cells and reagents can be transported on and off the chips within reasonable time periods (∼min). Our approach to measuring trap strength is similar to the one described above, where the fluid velocity necessary to break through a barrier is correlated to a barrier force [13, 62, 72]. This approach is also similar to those undertaken by the optical tweezer community, who calibrate their tweezers by measuring the escape velocity of trapped particles at various laser powers.

We have chosen to generalize this approach to allow for particles that may be near surfaces where Stokes drag is not strictly correct, where multipolar DEP forces may be important, and where electrode geometries may be complex [83]. In our initial validation of this approach, we were able to make absolute prediction of trap strength, as measured by the minimum volumetric flowrate needed for the particle to escape the trap. This volumetric flowrate can be related to a linear flowrate and then to a drag force using the analytical solutions for the drag on a stationary particle near a wall.

Our validation explained the non-intuitive trapping behavior of planar quadrupole traps (Figure 8.6), giving absolute agreement—to within 30%—between modeling and experiment with no fitting parameters [83]. We then extended this modeling to design a new, high-force trap created from extruded electrodes that could hold 13.2-μm beads with 95 pN of force at 2 V, and HL-60 cells with ∼60 pN of force at the same voltage [84, 85]. Again, we could make absolute predictions and verify them with experiments. We continue to extend this approach to design traps for different applications.

8.6. CONCLUSIONS

In conclusion, DEP traps, when properly confined, can be used to confine cells, acting as electrical tweezers. In this fashion cells can be positioned and manipulated in ways not achievable using other techniques, due to the dynamic nature of electric fields and the ability to shape the electrodes that create them.

Achieving a useful DEP system for manipulating cells requires an understanding of the forces present in these systems and an ability to model their interactions so as to predict the operating system conditions and whether they are compatible with cell health, etc. I have presented one approach to achieving these goals that employs quantitative modeling of these systems, along with examples of others who have sought to quantitate the performance of their systems.

8.7. ACKNOWLEDGEMENTS

The author wishes to thank Tom Jones for useful discussions and Thomas Schnelle for the some of the images in Figure 8.4. The author also wishes to acknowledge support from NIH, NSF, Draper Laboratories, and MIT for this work.

REFERENCES

Au: Provide article title.

[1] S. Archer, T.T. Li, A.T. Evans, S.T. Britland, and H. Morgan. *Biochem. Biophys. Res. Commun.*, 257:687, 1999.
[2] A. Ashkin. *Proc. Natl. Acad. Sci. U.S.A.*, 94:4853, 1997.
[3] A. Blake. *Handbook of Mechanics, Materials, and Structures.* Wiley, New York, 1985.
[4] R.H. Burdon. *Biochem. J.*, 240:313, 1986.
[5] S.W. Carper, J.J. Duffy, and E.W. Gerner. *Cancer Res.*, 47:5249, 1987.
[6] A. Castellanos, A. Ramos, A. Gonzalez, F. Morgan, and N. Green. *Proceedings of 14th International Conference on Dielectric Liquids 7–12 July 2002*. pp. 52, 2002.
[7] W.A. Catterall. *Ann. Rev. Biochem.*, 64:493, 1995.
[8] D.E. Chang, S. Loire, and I. Mezic. *J. Phys. D: Appl. Phys.*, 36:3073, 2003.
[9] C.F. Chou, J.O. Tegenfeldt, O. Bakajin, S.S. Chan, E.C. Cox, N. Darnton, T. Duke, and R.H. Austin. *Biophys. J.*, 83:2170, 2002.
[10] D.S. Clague and E.K. Wheeler. *Phys. Rev. E*, 64:026605, 2001.
[11] E.A. Craig. *CRC Crit. Rev. Biochem*., 18:239, 1985.
[12] A. Docoslis, N. Kalogerakis, and L.A. Behie. *Cytotechnology*, 30:133, 1999.
[13] M. Durr, J. Kentsch, T. Muller, T. Schnelle, and M. Stelzle. *Electrophoresis*, 24:722, 2003.
[14] S. Fiedler, S.G. Shirley, T. Schnelle, and G. Fuhr. *Anal. Chem.*, 70:1909, 1998.
[15] G. Fuhr, W.M. Arnold, R. Hagedorn, T. Muller, W. Benecke, B. Wagner, and U. Zimmermann. *Biochimi. Et. Biophys. Acta*, 1108:215, 1992a.
[16] G. Fuhr, H. Glasser, T. Muller, and T. Schnelle. *Biochimi. Et. Biophys. Acta-Gen. Sub.*, 1201:353, 1994.
[17] G. Fuhr, R. Hagedorn, T. Muller, W. Benecke, and B.Wagner. *J. Microelectromech. Sys.*, 1:141, 1992b.
[18] G. Fuhr, T. Schnelle, T. Muller, H. Hitzler, S. Monajembashi, and K.O. Greulich. *Appl. Phys. A-Mater. Sci. Process.*, 67:385, 1998.
[19] P. Ganatos, R. Pfeffer, and S. Weinbaum. *J. Fluid Mech.*, 99:755, 1980.
[20] P.R.C. Gascoyne and J. Vykoukal. *Electrophoresis*, 23:1973, 2002.
[21] P.R.C. Gascoyne, X.-B. Wang, Y. Huang, and F.F. Becker. *IEEE Trans. Ind. Appl.*, 33:670, 1997.
[22] P.R.C. Gascoyne, H. Ying, R. Pethig, J. Vykoukal, and F.F. Becker. *Measure. Sci. Technol.*, 3:439, 1992.
[23] W.J. Gibbs. *Conformal Transformations in Electrical Engineering.* Chapman & Hall, London, 1958.
[24] H. Glasser and G. Fuhr. *Bioelectrochem. Bioenerget.*, 47:301, 1998.
[25] H. Glasser, T. Schnelle, T. Muller, and G. Fuhr. *Thermochimi. Acta*, 333:183, 1999.
[26] A.J. Goldman, R.G. Cox, and H. Brenner. *Chem. Eng. Sci.*, 22:653, 1967.
[27] D.S. Gray, J.L. Tan, J. Voldman, and C.S. Chen. *Biosens. Bioelectron.*, 19:771, 2004.
[28] N.G. Green, A. Ramos, and H. Morgan. *J. Electrostat.*, 56:235, 2002.
[29] A.W. Griffith and J.M. Cooper. *Anal. Chem.*, 70:2607, 1998.
[30] A.J. Grodzinsky and M.L. Yarmush. Electrokinetic separations. In G. Stephanopoulus (ed.), *Bioprocessing*, Weinheim, Germany; New York, VCH, pp. 680, 1991.
[31] C. Grosse and H.P. Schwan. *Biophys. J.*, 63:1632, 1992.
[32] L.F. Hartley, K. Kaler, and R. Paul. *J. Electrostat.*, 46:233, 1999.
[33] Z. He. Nuclear instruments & methods in physics research, Section A accelerators, spectrometers, detectors and associated equipment, 365:572, 1995.
[34] Y. Huang, K.L. Ewalt, M. Tirado, T.R. Haigis, A. Forster, D. Ackley, M.J. Heller, J.P. O'Connell, and M. Krihak. *Anal. Chem.*, 73:1549, 2001.
[35] Y. Huang, R. Holzel, R. Pethig, and X.-B. Wang. *Phys. Med. Biol*., 37:1499, 1992.
[36] Y. Huang and R. Pethig. *Measure. Sci. Technol.,* 2:1142, 1991.
[37] Y. Huang, X.-B. Wang, F.F. Becker, and P.R.C. Gascoyne. *Biophys. J.*, 73:1118, 1997.
[38] M.P. Hughes. *Electrophoresis*, 23:2569, 2002.
[39] M.P. Hughes. *Nanoelectromechanics in Engineering and Biology*, CRC Press, Boca Raton, Fla., 2003.
[40] M.P. Hughes and H. Morgan. *J. Phys. D-Appl. Phys.*, 31:2205, 1998.
[41] M.P. Hughes and H. Morgan. *Biotechnol. Prog.*, 15:245, 1999.
[42] M.P. Hughes, H. Morgan, F.J. Rixon, J.P. Burt, and R. Pethig. *Biochim. Biophys. Acta*, 1425:119, 1998.
[43] A. Irimajiri, T. Hanai, and A. Inouye. *J. Theoret. Biol.*, 78:251, 1979.
[44] L.F. Jaffe and M.M. Poo. *J. Exp. Zool.*, 209:115, 1979.

[45] T.B. Jones. *Electromechanics of Particles.* Cambridge University Press, Cambridge, 1995.
[46] T.B. Jones. *IEEE Proc.-Nanobiotechnnol.*, 150:39, 2003.
[47] T.B. Jones and G.W. Bliss. *J. Appl. Phys.*, 48:1412, 1977.
[48] T.B. Jones, G.A. Kallio, and C.O. Collins. *J. Electrostat.*, 6:207, 1979.
[49] T.B. Jones and J.P. Kraybill. *J. Appl. Phys.*, 60:1247, 1986.
[50] T.B. Jones and M. Washizu. *J. Electrostat*., 33:199, 1994.
[51] T.B. Jones and M. Washizu. *J. Electrostat*., 37:121, 1996.
[52] D.R. Jung, R. Kapur, T. Adams, K.A. Giuliano, M. Mrksich, H.G. Craighead, and D.L. Taylor. *Crit. Rev. Biotechnol.*, 21:111, 2001.
[53] K.V.I.S. Kaler and T.B. Jones. *Biophys. J.*, 57:173, 1990.
[54] A. Lacy-Hulbert, J.C. Metcalfe, and R. Hesketh. *FASEB J.*, 12:395, 1998.
[55] S. Lindquist. *Annu. Rev. Biochem.*, 55:1151, 1986.
[56] N. Manaresi, A. Romani, G. Medoro, L. Altomare, A. Leonardi, M. Tartagni, and R. Guerrieri. *IEEE J. Solid-State Circ.*, 38:2297, 2003.
[57] G.H. Markx and C.L. Davey. *Enzyme Microb. Technol.*, 25:161, 1999.
[58] G.H. Markx, R. Pethig, and J. Rousselet. *J. Phys. D (Applied Physics)*, 30:2470, 1997.
[59] G.H. Markx, M.S. Talary, and R. Pethig. *J. Biotechnol.*, 32:29, 1994.
[60] H. Morgan and N.G. Green. *AC Electrokinetics: Colloids and Nanoparticles*. Research Studies Press, Baldock, Hertfordshire, England, 2003.
[61] H. Morgan, A.G. Izquierdo, D. Bakewell, N.G. Green, and A. Ramos. *J. Phys. D-Appl. Phys.*, 34:1553, 2001.
[62] T. Muller, G. Gradl, S. Howitz, S. Shirley, T. Schnelle, and G. Fuhr. *Biosens. Bioelectron.*, 14:247, 1999.
[63] M. Ozkan, T. Pisanic, J. Scheel, C. Barlow, S. Esener, and S.N. Bhatia. *Langmuir*, 19:1532, 2003.
[64] R. Pethig and D.B. Kell. *Phys. Med. Biol*., 32:933, 1987.
[65] C. Polk and E. Postow. *Handbook of Biological Effects of Electromagnetic Fields.* CRC Press, Boca Raton, FL, 1996.
[66] L. Qian, M. Scott, K.V.I.S. Kaler, and R. Paul. *J. Electrostat.*, 55:65, 2002.
[67] C. Reichle, T. Schnelle, T. Muller, T. Leya, and G. Fuhr. *Biochim. Et. Biophys. Acta-Bioenerg.*, 1459:218, 2000.
[68] T.A. Ryan, J. Myers, D. Holowka, B. Baird, and W.W. Webb. *Science*, 239:61, 1988.
[69] T. Schnelle, R. Hagedorn, G. Fuhr, S. Fiedler, and T. Muller. *Biochim. Et Biophys. Acta*, 1157:127, 1993.
[70] T. Schnelle, T. Muller, and G. Fuhr. *J. Electrostat.*, 46:13, 1999a.
[71] T. Schnelle, T. Muller, and G. Fuhr. *J. Electrostat.*, 50:17, 2000.
[72] T. Schnelle, T. Muller, G. Gradl, S.G. Shirley, and G. Fuhr. *J. Electrostat.*, 47:121, 1999b.
[73] H.P. Schwan. Dielectrophoresis and rotation of cells. In E. Neumann, A.E. Sowers, and C.A. Jordan, (eds.) *Electroporation and Electrofusion in Cell Biology*. New York, Plenum Press, pp. 3, 1989.
[74] H.P. Schwan. *Ann. Biomed. Eng.*, 20:269, 1992.
[75] J.R. Subjeck and T.T. Shyy. *Am. J. Physiol.*, 250:C1, 1986.
[76] J. Suehiro, R. Hamada, D. Noutomi, M. Shutou, and M. Hara. *J. Electrostat.*, 57:157, 2003.
[77] J. Suehiro and R. Pethig. *J. Phys. D-Appl. Phys.*, 31:3298, 1998.
[78] K. Svoboda and S.M. Block. *Ann. Rev. Biophys. Biomol. Struc.*, 23:247, 1994.
[79] T.Y. Tsong. *Biochim. et Biophys. Acta*, 1113:53, 1992.
[80] S. Tsukahara, T. Sakamoto, and H. Watarai. *Langmuir*, 16:3866, 2000.
[81] M. Urano and E.B. Douple. *Thermal effects on cells and tissues.* VSP, Utrecht, The Netherlands, 1988.
[82] P. Van Gerwen, W. Laureyn, W. Laureys, G. Huyberechts, M.O. De Beeck, K. Baert, J. Suls, W. Sansen, P. Jacobs, L. Hermans, and R. Mertens. *Sens. Actu. B-Chem.*, 49:73, 1998.
[83] J. Voldman, R.A. Braff, M. Toner, M.L. Gray, and M.A. Schmidt. *Biophys. J.*, 80:531, 2001.
[84] J. Voldman, M. Toner, M.L. Gray, and M.A. Schmidt. *Anal. Chem*., 74:3984, 2002.
[85] J. Voldman, M. Toner, M.L. Gray, and M.A. Schmidt. *J. Electrostat.* 57:69, 2003.
[86] X. Wang, X.-B. Wang, F.F. Becker, and P.R.C. Gascoyne. *J. Phys. D (Applied Physics)*, 29:1649, 1996.
[87] X. Wang, X.-B. Wang, and P.R.C. Gascoyne. *J. Electrostat*., 39:277, 1997a.
[88] X.-B. Wang, Y. Huang, P.R.C. Gascoyne, and F.F. Becker. *IEEE Trans. Ind. Appl.*, 33:660, 1997b.
[89] X.-B. Wang, Y. Huang, X. Wang, F.F. Becker, and P.R.C. Gascoyne. *Biophys. J.*, 72:1887, 1997c.
[90] X. J. Wang, J. Yang, and P.R.C. Gascoyne. *Biochimi. Et Biophys. Acta-Gen. Sub.*, 1426:53, 1999.
[91] M. Washizu and T.B. Jones. *J. Electrostat.*, 33:187, 1994.
[92] M. Washizu. and T. B. Jones. *J. Electrostat.*, 38:199, 1996.

[93] J.C. Weaver, T.E. Vaughan, and G.T. Martin. *Biophys. J.*, 76:3026, 1999.
[94] J. Wu. *J. Acoust. Soc. Am.*, 89:2140, 1991.
[95] G. Zhou, M. Imamura, J. Suehiro, and M. Hara. *Conference Record of the IEEE Industry Applications Conference*, 2:1404, 2002.
[96] X.F. Zhou, J.P.H. Burt, and R. Pethig. *Phys. Med. Biol.*, 43:1075, 1998.
[97] X.F. Zhou, G.H. Markx, and R. Pethig. *Biochim. Et Biophys. Acta-Biomem.*, 1281:60, 1996.
[98] U. Zimmermann. *Rev. Phys. Biochem. Pharma.*, 105:175, 1986.